Sensing-Communication Coexistence vs. Integration

Meng Liu, *Student Member, IEEE,* Minglei Yang, *Member, IEEE,* Zhaoming Zhang, Huifang Li, Fan Liu, *Member, IEEE*, Arumugam Nallanathan, *Fellow, IEEE*, and Lajos Hanzo, *Life Fellow, IEEE*

***Abstract*—The design options of sensing-communication coexistence (SCC) vs. integrated sensing and communications (ISAC) relying on non-orthogonal downlink transmission (NO-DLT) and transmit antenna selection are investigated. To be practical, both realistic residual hardware impairments (RHI) and imperfect successive interference cancellation are considered. The performance of the SCC and ISAC NO-DLT frameworks is characterized by deriving both the exact and the asymptotic outage probabilities (OPs) as well as the probability of successful target detection (PoD). Our numerical results demonstrate the accuracy of the theoretical analysis and confirm that: 1) The ISAC NO-DLT framework is superior to the SCC NO-DLT framework both in terms of its OP and PoD; 2) The realistic RHI degrades the S&C performance of both the SCC and ISAC NO-DLT frameworks.**

I. Introduction

Since the fifth-generation (5G) new radio (NR) standardization has reached maturity, the research commonly has turned to exploring new avenues. Sensing and communication (S&C) systems tend to become more and more similar in terms of their hardware, channel characteristics, and signal processing. Moreover, the combination of S&C can further improve the efficiency of wireless resources [1]. To this end, it is envisioned that radio sensing will develop into an essential function of the future communication systems in support of the vehicle-to-everything, smart homes, and environmental monitoring, etc [2]. Sensing-communication coexistence (SCC) as well as integrated sensing and communication (ISAC) are considered as feasible frameworks for the sixth-generation (6G) systems [3, 4].

Under the SCC framework, the S&C stations operate independently of each other, while in the ISAC framework, a unified hardware platform is used for accomplishing both S&C functionalities simultaneously [5–8]. In [5], a power allocation algorithm was designed for maximizing the communication throughput while satisfying the minimum receive signal-to-interference-plus-noise ratio (SINR) required for reliable sensing in the SCC system. The sum-rate and the probability of detection (PoD) for sensing were analyzed in the full-duplex SCC system scenario of [6]. In [7], the non-cooperative target was regarded as an illegal eavesdropper, and then both the receive signal-to-noise ratio (SNR) of the target and the secrecy rate of the system were investigated in the ISAC system, respectively. The authors of [8] derived both the sensing estimation rate and communications water-filling inner bound of the ISAC systems in which the sensing station was employed as a relay for communication.

The contributions [5–8] considered traditional orthogonal downlink transmission (O-DLT) for communication. However, O-DLT is unable to satisfy the massive access of requirements imposed by the rapids of Internet-of-Things (IoT) devices. As a remedy, non-orthogonal downlink transmission (NO-DLT) was proposed as a promising concept for 6G to ensure that the spectral efficiency and quality of service for the IoT devices can be further improved [9]. Specifically, NO-DLT provides services for multiple IoT devices by sending superimposed signals in the same time/frequency/code domain resources from the transmitter (TX). At the receiver (RX), typically successive interference cancelation (SIC) is adopted for detecting the signals [9]. In [10], the transmit beamformer was designed for maximizing the secrecy sum rate of ISAC NO-DLT systems, where the sensing target was considered to act as an eavesdropper degrading the confidentiality of the communication function. However, the authors of [5–8, 10] assumed having perfect radio frequency (RF) equipment, which is overly idealistic. In realistic practical scenarios, the equipment may be affected by phase noise, in-phase and quadrature-phase imbalance, and amplifier non-linearities. Although some advanced compensation algorithms have mitigated the influence of the hardware impairments (HIs), leaving solve residual HI (RHI) is inevitable [11].

The authors of [3–8] laid the solid foundations for both SCC and ISAC systems. However, the S&C performance analysis of the SCC and ISAC frameworks based on NO-DLT is still widely unexplored. In light of the above, we fill in these research gaps in the SCC and ISAC NO-DLT literature. As a further extension, a transmit antenna selection (TAS) strategy based on the IoT device fairness is proposed for reducing the number of activated RF chains and the power consumption as well as hardware cost, while maintaining the benefits of multiple antennas, while satisfying IoT devices having different priorities [12]. To be more practical, by taking into account the equipment aging and the environmental uncertainties, we elaborate on quantifying the residual hardware impairment (RHI) effects, which result in imperfect SIC (ipSIC) at the RXs. It should be emphasized that both the SCC and ISAC NO-DLT frameworks considered can be used in vehicle-to-vehicle and vehicle-to-everything communications [13, 14]. In order to evaluate the performance of the SCC and ISAC NO-DLT frameworks, the closed-form and approximate outage probabilities (OPs) of the IoT devices are obtained for communication. In addition, the sensing performance is analyzed by deriving the expression of the PoD. Our contributions are boldly and explicitly contrasted to the relevant state-of-the-art at a glance in Table I. Our numerical results show that due to the interference and other non-ideal factors, the OPs of the IoT devices exhibit error floors. Moreover, we demonstrate that the outage performance and the sensing capability of the ISAC outperform those of the SCC NO-DLT framework.

Notations: In this paper, $\mathcal{CN}(a, b)$ denotes a complex Gaussian random variable with mean a and variance b; $\mathbb{C}$

TABLE I: Comparison with available papers

Paper	[3]	[4]	[5]	[6]	[7]	[8]	Proposed
SCC		✓	✓	✓			✓
ISAC	✓	✓			✓	✓	✓
ISAC vs. SCC		✓					✓
RHI			✓				✓
PoD			✓				✓
OP							✓
NO-DLT							✓
TAS							✓

represent complex numbers; $\mathbb{E}[X]$ is the expectation of X; $\Gamma(a,b)$ represents the incomplete gamma function.

II. System Model

In Fig. 1(a) and Fig. 1(b), we consider the SCC and ISAC frameworks based on the NO-DLT supporting multiple IoT devices, respectively. For the SCC NO-DLT framework, the communication station S and the sensing station R operate independently of each other and are deployed at different locations. Specifically, S aims for communicating with N IoT devices $(D_1, D_2, \ldots, D_N)$, while R makes the decisions concerning the existence of a non-cooperative target T within the sensing range. It is assumed that all the IoT devices and R are equipped with a single-antenna, while S is equipped with N_S antennas with $N_S > N$. For notational convenience, we use $h_{S_kD_m}$ to denote the channel between the k-th antenna of S and the m-th IoT device. Furthermore, h_{RT} and h_{TR} denote the sensing channels of the $R \to T$ and $T \to R$ links, h_{RD_m} represents the interference channel spanning from R to the m-th IoT device, h_{S_kR} is the interference channel impinging from the k-th antenna of S upon R, and h_{TD_m} is the interference channel reflected from T to the m-th IoT device. By contrast, for the ISAC NO-DLT framework, S performs both communication and target sensing functions simultaneously. We assume that S is equipped with N_S antennas. Additionally, h_{S_kT} and h_{TS_k} denote the sensing channels and h_{SI} represents the self-interference (SI) channel associated with the transmitting and receiving signals simultaneously. It is assumed that the small-scale fading channels between all equipment pairs are modeled by the uncorrelated Rayleigh distribution. We use $h_i = h/\sqrt{1+d_i^{\alpha}}$ and $\rho_i = |h_i|^2$, $i \in \{S_kD_m, RT, TR, RD_m, TD_m, S_kR, S_kT, TS_k\}$ to denote the channel coefficients and gains, where $h \sim \mathcal{CN}(0,\Omega)$. Finally, α is the path-loss exponent and d_i denotes the distance[1].

For the TAS strategy proposed, the best antenna is selected for maximizing the received SINR of D_m. More particularly, to further improve the fairness of the IoT devices for the NO-DLT system considered, we assume that the farthest IoT device D_N has the highest priority, followed by D_{N-1}, ..., while D_1 has the lowest priority. On this basis, the best antenna for D_N is selected from N_S antennas, ..., and D_1 selects from the remaining $N_S - N + 1$ antennas. Hence, the best antenna for D_m can be chosen as

$$k^* = \arg \max_{k \in \{1,2,\ldots,N_S-N+m\}} \rho_{S_kD_m} \tag{1}$$

A. SCC NO-DLT framework

As seen from Fig. 1(a) for the SCC NO-DLT framework, S and R transmit their own signals so that the S&C can be carried out. As for the communication function, S intends to send $x_S = \sum_{n=1}^{N} \sqrt{a_n P_S} x_n$ to the IoT devices, where $x_n \in \mathbb{C}$ is the expected signal of D_n with $\mathbb{E}\left[|x_n|^2\right] = 1$, P_S denotes the transmit power of S, and a_n represents the power allocation coefficient of x_n with $\sum_{n=1}^{N} a_n = 1$ and $a_1 < a_2 < \ldots < a_N$. As for the sensing function, R sends $x_R = \sqrt{P_R} x_r$ to sense the non-cooperative targets, where $x_r \in \mathbb{C}$ is the sensing signal with $\mathbb{E}\left[|x_r|^2\right] = 1$ and P_R denotes the transmit power of R. From a global perspective, the signal received at the m-th IoT device is expressed as[2]

$$\begin{aligned} y_{D_m}^{\mathrm{C}} = & h_{SD_m}(x_S + \eta_{t,SD_m}) + h_{TD_m} h_{RT}(\delta_{RD_m} x_R + \eta_{t,RD_m}) \\ & + \eta_{r,SD_m} + \eta_{r,RD_m}^{T} + h_{RD_m}(x_R + \eta_{t,RD_m}) + \eta_{r,RD_m}^{R} + n_{D_m}^{\mathrm{C}}, \end{aligned} \tag{2}$$

where δ_{RD_m} is the scattering coefficient of the target by $R \to T \to D_m$[3], $n_{D_m}^{\mathrm{C}} \sim \mathcal{CN}(0, N_0)$ denotes the additive white Gaussian noise (AWGN) at D_m and N_0 is the noise power. Furthermore, $\eta_{t,SD_m} \sim \mathcal{CN}\left(0, \kappa_{t,S}^2 P_S\right)$ and $\eta_{r,SD_m} \sim \mathcal{CN}\left(0, \kappa_{r,D_m}^2 \rho_{SD_m} P_S\right)$ represent the distortion of S and D_m by $S \to D_m$, while $\kappa_{t,S}$ and κ_{r,D_m} characterize the levels of RHI at the TX and RX. To elaborate further, $\eta_{t,RD_m} \sim \mathcal{CN}\left(0, \kappa_{t,S}^2 P_R\right)$ and $\eta_{r,RD_m}^{T} \sim \mathcal{CN}\left(0, \kappa_{r,D_m}^2 \rho_{RT} \rho_{TD_m} P_R\right)$ represent the distortion of R and D_m by $R \to T \to D_m$ and $\eta_{r,RD_m}^{R} \sim \mathcal{CN}\left(0, \kappa_{r,D_m}^2 \rho_{RD_m} P_R\right)$ represents the distortion of D_m by $R \to D_m$ [11]. After some further mathematical manipulations, (2) can be rewritten as

$$\begin{aligned} y_{D_m}^{\mathrm{C}} = & \underbrace{h_{SD_m}(x_S + \eta_{SD_m})}_{\text{Signal from } S} + \underbrace{h_{RD_m}(x_R + \eta_{RD_m})}_{\text{Interference from } R} \\ & + \underbrace{h_{TD_m} h_{RT}(\delta_{RD_m} x_R + \eta_{RD_m})}_{\text{Interference from } T} + n_{D_m}^{\mathrm{C}}, \end{aligned} \tag{3}$$

where $\eta_{SD_m} \sim \mathcal{CN}\left(0, \kappa_{SD_m}^2 P_S\right)$ and $\eta_{RD_m} \sim \mathcal{CN}\left(0, \kappa_{RD_m}^2 P_R\right)$ are the aggregate levels of RHI with $\kappa_{SD_m} = \sqrt{\kappa_{t,S}^2 + \kappa_{r,D_m}^2}$ and $\kappa_{RD_m} = \sqrt{\kappa_{t,R}^2 + \kappa_{r,D_m}^2}$.

According to the NO-DLT protocol, SIC is adopted at the RXs for detecting the signals.[4] Therefore, the received SINR of x_j at D_m, $m \leqslant j \leqslant N$, can be expressed as

$$\gamma_{D_{m\to j}}^{\mathrm{C}} = \frac{\rho_{SD_m} a_j \gamma_S}{\rho_{SD_m} \gamma_S \phi_1 + \rho_{RD_m} \gamma_R \phi_2 + \rho_{RT} \rho_{TD_m} \gamma_R \phi_3 + 1}, \tag{4}$$

where $\rho_{SD_m} \gamma_S \phi_1$ represents the inter-user interference with $\phi_1 = \sum_{n=1}^{j-1} a_n + \varepsilon \sum_{p=j+1}^{N} a_p + \kappa_{SD_m}^2$, $\rho_{RD_m} \gamma_R \phi_2$ denotes the interference caused by R in conjunction with

[1] In essence, the channel models of S&C are distinct. Explicitly, during the signal transmission, the communication channel is unidirectional, while the bidirectional sensing channel is multiplicative, which can be expressed as $h_{RT}h_{TR}$ and $h_{ST}h_{TS}$ for the SCC and ISAC frameworks, respectively. It should be further noted that if there is no target in the sensing range, then h_{RT}, h_{TR}, and h_{TD_m} are set to 0. If the target is sensed by R, the channel state information (CSI) can be estimated from the receive signals, which will be discussed in Section IV in detail.

[2] Hereinafter, to simplify the statement, $h_{S_k^*D_m}$, $h_{S_k^*R}$, $h_{S_k^*T}$, and $h_{TS_k^*}$ are replaced by h_{SD_m}, h_{SR}, h_{ST} and h_{TS}, respectively.

[3] It should be pointed out that the scattering coefficient is affected by target structure, surface medium, signal wavelength, polarization mode and target azimuth angle [15].

[4] Note that although the SIC increases the complexity of the RXs, with the development of industrial technology, more and more sophisticated and powerful high-end IoT devices will be designed, which facilitates the successful execution of SIC.

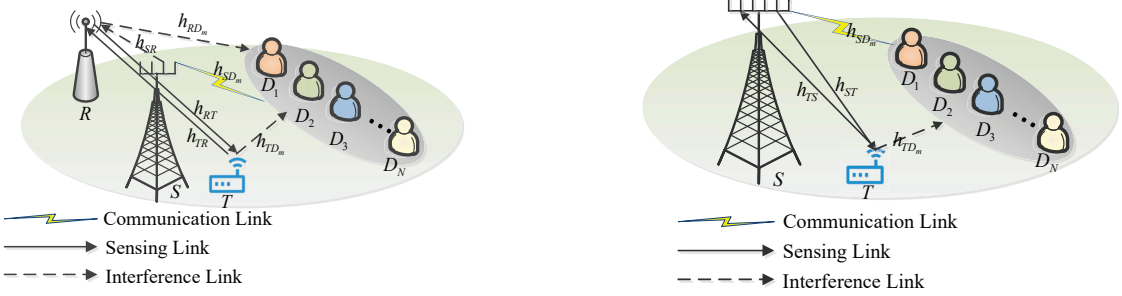

(a): An illustration of the SCC NO-DLT framework. (b): An illustration of the ISAC NO-DLT framework.

Fig. 1: System model.

$\phi_2 = 1+\kappa_{RD_m}^2$, $\rho_{RT}\rho_{TD_m}\gamma_R\phi_3$ is the interference caused by the target scattering along with $\phi_3 = \delta_{RD_m}^2 + \kappa_{RD_m}^2$, $\gamma_S = P_S/N_0$, $\gamma_R = P_R/N_0$, and $\varepsilon \in [0,1]$ represents the level of SIC.

Similar to (3), the signal received at R can be expressed as

$$y_R^{\mathrm{C}} = \underbrace{h_{TR}h_{RT}\left(\delta_{RR}x_R + \eta_{RR}\right)}_{\text{Echo from } T} + \underbrace{\sum h_{SR}\left(x_S + \eta_{SR}\right)}_{\text{Interference from } S} + n_R^{\mathrm{C}}, \tag{5}$$

where $\eta_{RR} \sim \mathcal{CN}\left(0, \kappa_{RR}^2 P_R\right)$ and $\eta_{SR} \sim \mathcal{CN}\left(0, \kappa_{SR}^2 P_S\right)$ are the aggregated RHI caused by $R \to T \to R$ and $S \to R$. δ_{RR} is the scattering coefficient of the target by $R \to T \to R$, and $n_R^{\mathrm{C}} \sim \mathcal{CN}\left(0, N_0\right)$ denotes the AWGN at R.

B. ISAC NO-DLT framework

As seen from Fig. 1(b) for the ISAC NO-DLT framework, the signal transmitted by S is capable of simultaneously supporting C&S. Explicitly, S transmits $x_S = \sum_{n=1}^{N}\sqrt{a_n P_S}x_n$ to communicate with N IoT devices and concomitantly sense the non-cooperative targets. Therefore, the signal received at the m-th IoT device can be expressed as[5]

$$y_{D_m}^{\mathrm{I}} = \underbrace{\sum h_{TD_m}h_{ST}(\delta_{SD_m}x_S + \eta_{SD_m})}_{\text{Interference from } T} + \underbrace{h_{SD_m}(x_S + \eta_{SD_m})}_{\text{Signals from } S} + n_{D_m}^{\mathrm{I}}, \tag{6}$$

where δ_{SD_m} denotes the scattering coefficient of the target in the $S \to T \to D_m$ links, and $n_{D_m}^{\mathrm{I}} \sim \mathcal{CN}\left(0, N_0\right)$ is the AWGN at D_m.

According to the NO-DLT protocol, the SINR at D_m, $m \leqslant j \leqslant N$, can be expressed as

$$\gamma_{D_{m\to j}}^{\mathrm{I}} = \frac{\rho_{SD_m}a_j\gamma_S}{\rho_{SD_m}\gamma_S\phi_1 + \rho_{TD_m}\rho_{ST}\gamma_S\phi_4 + 1}, \tag{7}$$

where we have $\phi_4 = N\left(\delta_{SD_m}^2 + \kappa_{SD_m}^2\right)$.

The signal received at S can be formulated as

$$y_S^{\mathrm{I}} = \sum h_{TS}h_{ST}\left(\delta_{RR}x_S + \eta_{SS}\right) + h_{SI}\sqrt{P_S}x_{SI} + n_S^{\mathrm{I}}, \tag{8}$$

where denotes the AWGN at S, $x_{SI} \in \mathbb{C}$ denotes the SI signal associated with $\mathbb{E}\left[|x_{SI}|^2\right] = 1$, $\eta_{SS} \sim \mathcal{CN}\left(0, \kappa_{SS}^2 P_S\right)$ and δ_{SS} represents the aggregated RHI and scattering coefficient of the target caused by $S \to T \to S$, respectively.

[5]We need to point that the expected signals of the IoT devices exist in the echo, while the channels h_{ST} and h_{TD_m} need to be estimated, which has exceeded the scope of this treatise and will be set aside for our future work.

III. Communication Performance Analysis

In this section, both the exact and asymptotic OPs are analyzed to evaluate the communication performance.

A. Exact OP

1) SCC NO-DLT framework: The outage event occurs at the m-th IoT device, when the expected signal of D_j cannot be decoded by D_m, $m \leqslant j \leqslant N$. Thus, the OP of D_m for the SCC framework can be expressed as

$$\mathrm{P}_{D_m}^{\mathrm{C}} = 1 - \Pr\left(\gamma_{D_{m\to m}}^{\mathrm{C}} > \gamma_{thm}, \ldots, \gamma_{D_{m\to M}}^{\mathrm{C}} > \gamma_{thM}\right), \tag{9}$$

where γ_{thj} denotes the outage threshold SINR of D_j.

Based on the above, we derive the exact OP expression $\mathrm{P}_{D_m}^{\mathrm{C}}$ for the SCC NO-DLT framework in the following theorem.

Theorem 1. *For the SCC framework,* $\mathrm{P}_{D_m}^{\mathrm{C}}$ *is given by*

$$\mathrm{P}_{D_m}^{\mathrm{C}} = 1 - \sum_{t=1}^{N_S-N+m}\binom{N_S-N+m}{t}(-1)^t e^{\frac{\beta_{SD_m}}{t\vartheta\phi_3\beta_{TD_m}\beta_{RT}} - \frac{\varphi_m^* t}{\beta_{SD_m}}} \times \frac{\beta_{SD_m}^2}{t\vartheta\phi_3\beta_{TD_m}\beta_{RT}(\beta_{SD_m} + t\vartheta\phi_1\beta_{RD_m})}\Gamma\left(0, \frac{\beta_{SD_m}}{t\vartheta\phi_3\beta_{TD_m}\beta_{RT}}\right), \tag{10}$$

where we have $\beta_i = \Omega/\sqrt{1+d_i^{\alpha}}$, $\varphi_m^* = \max_{m\leqslant j\leqslant N}\varphi_j$, $\vartheta = \varphi_m^*\gamma_R$, *and* $\varphi_j = \gamma_{thj}/[\gamma_S\left(a_j - \gamma_{thj}\phi_1\right)]$ *with* $a_j > \gamma_{thj}\phi_1$, *otherwise* $\mathrm{P}_{D_m}^{\mathrm{C}} = 1$.

Proof. See Appendix. □

2) ISAC NO-DLT framework: Similar to (9), the OP of D_m for the ISAC NO-DLT framework is described as

$$\mathrm{P}_{D_m}^{\mathrm{I}} = 1 - \Pr\left(\gamma_{D_{m\to m}}^{\mathrm{I}} > \gamma_{thm}, \ldots, \gamma_{D_{m\to M}}^{\mathrm{I}} > \gamma_{thM}\right). \tag{11}$$

Based on the above, we derive the exact OP expression $\mathrm{P}_{D_m}^{\mathrm{I}}$ for the ISAC NO-DLT framework in the following theorem.

Theorem 2. *For the ISAC framework,* $\mathrm{P}_{D_m}^{\mathrm{I}}$ *is given by*

$$\mathrm{P}_{D_m}^{\mathrm{I}} = 1 - \sum_{q=1}^{N_S-N+m}\binom{N_S-N+m}{q}(-1)^{q+1}\frac{\beta_{SD_m}}{q\xi\phi_4\beta_{ST}\beta_{TD_m}} \times e^{\frac{\beta_{SD_m}}{q\xi\phi_4\beta_{ST}\beta_{TD_m}} - \frac{q\theta_m^*}{\beta_{SD_m}}}\Gamma\left(0, \frac{\beta_{SD_m}}{q\xi\phi_4\beta_{ST}\beta_{TD_m}}\right), \tag{12}$$

where we have $\theta_m^* = \max_{m\leqslant j\leqslant N}\theta_j$, $\xi = \gamma_S\theta_m^*$, *and* $\theta_j = \gamma_{thj}/(a_j - \gamma_{thj}\phi_1)$ *with* $a_j > \gamma_{thj}\phi_1$, *otherwise* $\mathrm{P}_{D_m}^{\mathrm{I}} = 1$.

Proof. Similar to Theorem 1, substituting (7) into (11), (12) can be obtained after some mathematical manipulations. □

B. Asymptotic OP

1) SCC NO-DLT framework: When $\gamma_S, \gamma_R \to \infty$, the SINR of x_j at D_m can be rewritten according to (4) as

$$\gamma^{\mathrm{C},\infty}_{D_{m\to j}} = \frac{\rho_{SD_m} a_j}{\rho_{SD_m}\phi_1 + \rho_{RD_m}\phi_2 + \rho_{RT}\rho_{TD_m}\phi_3}. \tag{13}$$

The asymptotic OP expression of D_m for the SCC NO-DLT framework is given in the following corollary.

Corollary 1. *The asymptotic analytical OP expression of D_m for the SCC NO-DLT framework is given by*

$$\mathrm{P}^{\mathrm{C},\infty}_{D_m} = 1 - \sum_{t=1}^{N_S-N+m} \binom{N_S-N+m}{t} (-1)^{t+1} e^{\frac{\beta_{SD_m}}{\beta_{TD_m}\beta_{RT} t\phi_3 \varphi^*_{m,\infty}}} \times \frac{\beta^2_{SD_m}}{\beta_{RT}\beta_{TD_m} t\phi_3 \varphi^*_{m,\infty}\left(\beta_{SD_m} + t\phi_2\varphi^*_{m,\infty}\beta_{RD_m}\right)} \times \Gamma\left(0, \frac{\beta_{SD_m}}{\beta_{TD_m}\beta_{RT} t\phi_3\varphi^*_{m,\infty}}\right), \tag{14}$$

where we have $\varphi^*_{m,\infty} = \max\limits_{m\leqslant j\leqslant N} \varphi_{j,\infty}$ with $\varphi_{j,\infty} = \varphi_j\gamma_S$.

Proof. Substituting (13) into (9), similar to Theorem 1, (14) can be obtained after some mathematical manipulations. □

2) ISAC NO-DLT framework: When $\gamma_S, \gamma_R \to \infty$, the SINR of x_j at D_m can be rewritten according to (7) as

$$\gamma^{\mathrm{I},\infty}_{D_{m\to j}} = \frac{\rho_{SD_m} a_j}{\rho_{SD_m}\phi_1 + \rho_{ST}\rho_{TD_m}\phi_4}. \tag{15}$$

The asymptotic expression OP of D_m for the ISAC NO-DLT framework is given in the following corollary.

Corollary 2. *The asymptotic analytical OP expression of D_m for the ISAC NO-DLT framework is expressed as*

$$\mathrm{P}^{\mathrm{I},\infty}_{D_m} = 1 - \sum_{q=1}^{N_S-N+m} \binom{N_S-N+m}{q} (-1)^{q+1} e^{\frac{\beta_{SD_m}}{q\beta_{TD_m}\beta_{ST}\phi_4\theta^*_m}} \times \frac{\beta_{SD_m}}{q\phi_4\theta^*_m\beta_{TD_m}\beta_{ST}} \Gamma\left(0, \frac{\beta_{SD_m}}{q\beta_{TD_m}\beta_{ST}\phi_4\theta^*_m}\right). \tag{16}$$

Remark 1. *It should be pointed out that the outage performance of the IoT devices is related to the target attributes. If the target is absent, both the SCC and ISAC NO-DLT frameworks degenerate into the traditional NO-DLT frameworks. Moreover, if $\kappa_{SD_m} = \kappa_{RD_m} = \kappa_{RR} = \kappa_{SR} = \kappa_{SS} = \varepsilon = 0$ is established, the frameworks reduce to the ideal condition.*

IV. Sensing Performance Analysis

For sensing, the fundamental tasks are target detection and parameter estimation. Specifically, target detection implies that the sensing RXs determine whether the target is present or not based on the power of the received signals. By contrast, parameter estimation is used to judge the target attributes, such as velocity and distance, based on the delay or Doppler frequency of the received signals. Hence, target detection is the premise of parameters estimation. Therefore, in this paper, we focus our attention on the problem of target detection. During the signal processing, due to the noise and the interference from S, the sensing RXs may make wrong decisions, which is reflected in the sensing performance of the system. Indeed, typically the PoD and probability of false alarm (PoFA) are used to jointly describe the sensing performance [15]. The PoD $\mathrm{P_d}$ and the PoFA $\mathrm{P_{fa}}$ represent the probability of the sensing equipment making a correct or incorrect decisions when the target is within the sensing range. Specifically, $\mathrm{P_d}$ and $\mathrm{P_{fa}}$ are respectively given as $\mathrm{P_d} = \Pr(H_1|H_1)$ and $\mathrm{P_{fa}} = \Pr(H_1|H_0)$, where the alternative hypothesis H_1 refers to the receive signals containing echoes, noise, and interference. By contrast, the null hypothesis H_0 indicates that the receive signals do not contain echoes [15]. Based on this, we now study the sensing behavior by deriving the PoDs for the SCC and ISAC NO-DLT frameworks.

A. SCC NO-DLT framework

For the SCC NO-DLT framework, we assume that the null hypothesis H^{C}_0 only includes the AWGN and the interference from S, while the alternative hypothesis H^{C}_1 additionally includes the target echoes. According to (5), the binary hypothesis sensing problem may be described as

$$H^{\mathrm{C}}_0 : y^{\mathrm{C}}_R = \sum h_{SR}\left(x_S + \eta_{SR}\right) + n^{\mathrm{C}}_R, \tag{17}$$
$$H^{\mathrm{C}}_1 : y^{\mathrm{C}}_R = h_{TR}h_{RT}(\delta_{RR}x_R + \eta_{RR}) + \sum h_{SR}(x_S + \eta_{SR}) + n^{\mathrm{C}}_R.$$

From (17), we can observe that the power received at R is

$$\mathbb{E}\left[\left|y^{\mathrm{C}}_R\right|^2\right] = \rho_{RT}\rho_{TR}P_R\left(\delta^2_{RR} + \kappa^2_{RR}\right) + N\rho_{SR}\left(1+\kappa^2_{SR}\right)P_S + N_0. \tag{18}$$

Then, the information related to the target for the SCC framework may be inferred as

$$\rho_{RT}\rho_{TR}\left(\delta^2_{RR} + \kappa^2_{RR}\right)P_R = \mathbb{E}\left[\left|y^{\mathrm{C}}_R\right|^2\right] - N\rho_{SR}\left(1+\kappa^2_{SR}\right)P_S - N_0. \tag{19}$$

It should be noted that the noise and channels in (19) obey the Gaussian and Rayleigh distributions under statistical theory. However, due to the randomness of the instantaneous noise and channels, it is possible to make the wrong decision by the sensing RX. Therefore, according to the Neyman-Pearson criterion [15], the PoD may be maximized at a fixed PoFA. Based on (17), we can confirm that $\mathbb{E}\left[\left|y^{\mathrm{C}}_R\right|^2\right]$ is the non-central Chi-square random variable with a degree-of-freedoms (DoF) which is three under H^{C}_0 and five under H^{C}_1. Hence, the false-alarm and sensing probabilities of R are respectively expressed as

$$\mathrm{P^C_{fa}} = Q_{\frac{3}{2}}\left(\sqrt{2N\rho_{SR}P_S\left(1+\kappa^2_{SR}\right)/N_0}, \sqrt{2\zeta/N_0}\right), \tag{20}$$

$$\mathrm{P^C_d} = Q_{\frac{5}{2}}\left(\sqrt{2(\rho_{RT}\rho_{TR}\delta^2_{RR}P_R + N\rho_{SR}P_S)/P^{\mathrm{C}}_{\mathrm{n}}}, \sqrt{2\zeta/P^{\mathrm{C}}_{\mathrm{n}}}\right), \tag{21}$$

where we have $P^{\mathrm{C}}_{\mathrm{n}} = \rho_{RT}\rho_{TR}\kappa^2_{RR}P_R + N\rho_{SR}\kappa^2_{SR}P_S + N_0$, ζ denotes the sensing threshold and $Q(\cdot,\cdot)$ is the Marcum Q-function.

B. ISAC NO-DLT framework

For the ISAC NO-DLT framework, assuming that the null hypothesis H_0^{I} only includes the noise and SI from S, while the alternative hypothesis H_1^{I} is additionally contaminated by the target echoes. According to (8), we arrive at

$$H_0^{\mathrm{I}}: y_S^{\mathrm{I}} = \sum h_{SI}\sqrt{P_S}x_{SI} + n_S^{\mathrm{I}}, \tag{22}$$
$$H_1^{\mathrm{I}}: y_S^{\mathrm{I}} = \sum h_{TS}h_{ST}\left(\delta_{RR}x_S + \eta_{SS}\right) + h_{SI}\sqrt{P_S}x_{SI} + n_S^{\mathrm{I}}.$$

Similar to (19), the information related to the target in the ISAC framework may be expressed as

$$N\rho_{ST}\rho_{TS}\left(\delta_{SS}^2+\kappa_{SS}^2\right)P_S = \mathbb{E}\left[\left\|y_S^{\mathrm{I}}\right\|^2\right] - N\rho_{LI}P_S - N_0. \tag{23}$$

From (22), we can observe that the receive power of S is a non-central Chi-square random variable with a DoF which is two under H_0^{I} and four under H_1^{I}. Thus, the false-alarm and the correct PoD of S are respectively expressed as

$$\mathrm{P}_{\mathrm{fa}}^{\mathrm{I}} = Q_1\left(\sqrt{2NP_S\rho_{SI}/N_0}, \sqrt{2\zeta/N_0}\right), \tag{24}$$
$$\mathrm{P}_{\mathrm{d}}^{\mathrm{I}} = Q_2\left(\sqrt{2NP_S(\delta_{SS}^2\rho_{ST}\rho_{TS}+\rho_{SI})/P_{\mathrm{n}}^{\mathrm{I}}}, \sqrt{2\zeta/P_{\mathrm{n}}^{\mathrm{I}}}\right), \tag{25}$$

where we have $P_{\mathrm{n}}^{\mathrm{I}} = N\kappa_{SS}^2\rho_{ST}\rho_{TS}P_S + N_0$.

Remark 2. *From (20), (21), (24), and (25), we can observe that for a given false-alarm probability, there exists a unique ζ corresponding to it, and then the PoD can be obtained. Additionally, it can be concluded that the PoFA is caused by the combination of the AWGN and the interference imposed by the communication TX on the sensing RX.*

V. Numerical Results

In this section, some numerical results are provided for characterizing the accuracy of the theoretical analysis by Monte-Carlo computer simulations. According to the third generation partnership (3GPP) LTE-advanced [16] and practical communication scenarios, e.g., vehicle-to-vehicle communication in urban environment, and low-altitude unmanned aerial vehicle communication are used, which have the simulation parameters of Table II.[6]

TABLE II: Simulation parameters

Parameter	Value	Parameter	Value	Parameter	Value
κ	0.08	ε	0.01	N_0	1
N	2	a_1	0.3	a_2	0.7
γ_{th1}	1	γ_{th2}	2	Ω	1
α	2	δ_{RD_m}, δ_{SD_m}	0.1	δ_{SS}, δ_{RR}	0.9
d_{SR}, d_{SD_1}	10 m	d_{SD_2}, d_{RD_1}	15 m	d_{RT}, d_{TR}	15 m
d_{ST}, d_{TS}	15 m	d_{RD_2}, d_{TD_1}	20 m	d_{TD_2}	25 m

Fig. 2 illustrates the OPs of the IoT devices versus the transmit power of the communication station both for the ISAC and SCC frameworks at the same power consumption. The perfect match between our Monte Carlo simulation results and the theoretical values confirms the accuracy of the theoretical derivation in Section III. Observe from Fig. 2 that the proposed NO-DLT frameworks deliver exceptional outage performance compared to the traditional O-DLT. It can be further observed that the ISAC NO-DLT framework outperforms the SCC NO-DLT framework. This is because for the SCC framework, the direct irradiation of the sensing station may impose strong interference on the IoT devices, while the ISAC framework avoids this phenomenon. Additionally, we can also observe that the OPs of the IoT devices are bounded by the non-ideal factors of RHI, ipSIC as well as the interference among the equipment.

[6]In contrast to [14] and [17], the main objective of this paper is to compare the performance of SCC and ISAC frameworks, so as to provide theoretical support for the design of future S&C systems. Using real-world data is set aside for a full future journal paper.

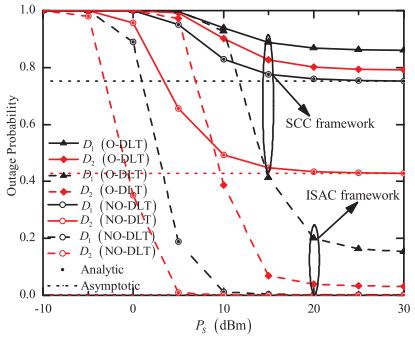

Fig. 2: OP vs. the power of communication station.

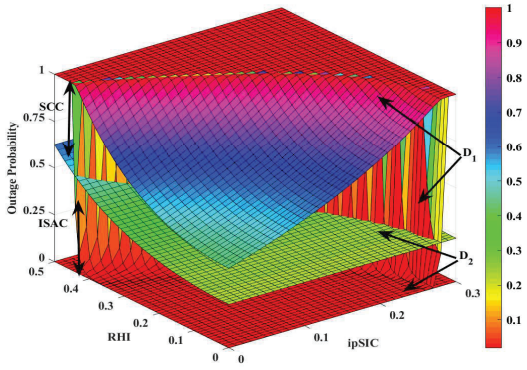

Fig. 3: OP vs. κ and ε.

Fig. 3 presents the OPs of the IoT devices versus the RHI and ipSIC at $P_S = P_R = 30$ dBm and $P_S = 60$ dBm for the SCC and ISAC frameworks, respectively. It can be seen that both the ipSIC and RHI degrade the outage performance of the IoT devices, and that the OPs are more sensitive to the performance of SIC than to the RHI. Furthermore, since the signal detection at the farthest IoT device is independent of the SIC performance, the variations of the ipSIC parameters have no effect on the OP of D_N.

Fig. 4(a) shows the PoD versus the transmit power of the sensing station at $\mathrm{P}_{\mathrm{fa}} = 10^{-6}$. We plot the PoD curves for both the SCC and ISAC frameworks of three scenarios: 1) Fixed $P_S = 20$ dBm; 2) Fixed $P_S = 0$; 3) $P_S = P_R$. Due to the absence of the interference from the communication station, the sensing performance of the ISAC framework is superior to the SCC framework. Moreover, when $P_S = 0$, the SCC framework transforms into a pure sensing framework, and the sensing capabilities of the SCC and ISAC frameworks are close to each other. Fig. 4(b) depicts the PoD versus the

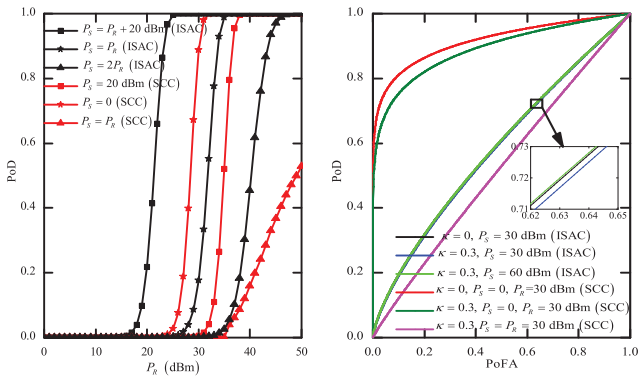

(a) (b)

Fig. 4: (a) $\mathrm{P_d}$ vs. the power of sensing station; (b) $\mathrm{P_d}$ vs. $\mathrm{P_{fa}}$.

false-alarm probability of the sensing station. In other words, the sensing behavior is represented by the receiver's operating characteristic (ROC) curves. For the SCC framework, the interference arriving from the communication station is absent when $P_S = 0$. In this case, the area under the curve (AUC) reaches its maximum and the framework has excellent sensing performance. When $P_R = P_S$, the sensing performance is gravely eroded by the communication station, resulting in an almost linear relationship between $\mathrm{P_d}$ and $\mathrm{P_{fa}}$. Observe for the ISAC framework that the AUCs remain almost constant vs. the RHI and vs. the transmit power of the communication station, which indicates that the ISAC framework exhibits excellent robustness. Finally, as expected, the RHI degrades the sensing performance of the frameworks.

VI. Conclusions

In this paper, the performance of the SCC and ISAC NO-DLT TAS frameworks was investigated from S&C. The exact and the asymptotic OPs and the PoD were derived in the context of RHI and ipSIC. The simulation results showed that the ISAC framework is superior to the SCC framework in terms of its outage and sensing performance at the same power consumption. Naturally, the RHI degrades both the SCC and ISAC performance.

Appendix: Proof of Theorem 1

In the following, we first derive the cumulative distribution function (CDF) of the channel gains between the selected antenna and D_m.

By using the order statistics method, the CDF of ρ_{SD_m} is given by

$$F_{\rho_{SD_m}}(x) = \sum_{l=0}^{N_S-m} \binom{N_S-m}{l} (-1)^l e^{-\frac{lx}{\beta_{SD_m}}}. \quad \text{(A.1)}$$

Substituting (4) into (9), after some mathematical manipulations, the OP of D_m may be formulated as

$$\begin{aligned}\mathrm{P}^{\mathrm{I}}_{D_m} &= 1-\Pr\left(\rho_{SD_m} > \varphi^*_m\left(\rho_{RD_m}\gamma_R\phi_2+\rho_{RT}\rho_{TD_m}\gamma_R\phi_3+1\right)\right)\\ &= 1-\int_{\varphi^*_m(x\gamma_R\phi_2+yz\gamma_R\phi_3+1)}^{\infty} f_{\rho_{SD_m}}(w)\int_0^{\infty} f_{\rho_{RD_m}}(x)\\ &\quad\times\int_0^{\infty} f_{\rho_{RT}}(y)\int_0^{\infty} f_{\rho_{TD_m}}(z)dwdxdydz. \quad \text{(A.2)}\end{aligned}$$

By using the probability density function of the Rayleigh fading channels, (A.2) may be further expressed as

$$\begin{aligned}\mathrm{P}^{\mathrm{I}}_{D_m} &= 1-\int_0^{\infty}\int_0^{\infty}\int_0^{\infty}\frac{1}{\beta_{RD_m}\beta_{RT}\beta_{TD_m}}e^{-\frac{x}{\beta_{RD_m}}-\frac{y}{\beta_{RT}}-\frac{z}{\beta_{TD_m}}}\\ &\quad\times F_{\rho_{SD_m}}\left(\varphi^*_m\left(x\gamma_R\phi_2+yz\gamma_R\phi_3+1\right)\right)dxdydz. \quad \text{(A.3)}\end{aligned}$$

With the aid of (A.1) and [18, Eq. (3.462.15)], (10) can be obtained after some further mathematical manipulations.

References

[1] Y. Cui, F. Liu, X. Jing, and J. Mu, "Integrating sensing and communications for ubiquitous IoT: Applications, trends, and challenges," *IEEE Netw.*, vol. 35, no. 5, pp. 158–167, 2021.

[2] F. Liu, Y. Cui, C. Masouros, J. Xu, T. X. Han, Y. C. Eldar, and S. Buzzi, "Integrated sensing and communications: Toward dual-functional wireless networks for 6G and beyond," *IEEE J. Sel. Areas Commun.*, vol. 40, no. 6, pp. 1728–1767, Jun. 2022.

[3] F. Liu, C. Masouros, A. P. Petropulu, H. Griffiths, and L. Hanzo, "Joint radar and communication design: Applications, state-of-the-art, and the road ahead," *IEEE Trans. Commun.*, vol. 68, no. 6, pp. 3834–3862, Jun. 2020.

[4] F. Liu, C. Masouros, A. Li, H. Sun, and L. Hanzo, "MU-MIMO communications with MIMO radar: From co-existence to joint transmission," *IEEE Trans. Wireless Commun*, vol. 17, no. 4, pp. 2755–2770, Feb. 2018.

[5] F. Wang and H. Li, "Power allocation for coexisting multicarrier radar and communication systems in cluttered environments," *IEEE Trans. Signal Process.*, vol. 69, pp. 1603–1613, Feb. 2021.

[6] S. Biswas, K. Singh, O. Taghizadeh, and T. Ratnarajah, "Design and analysis of FD MIMO cellular systems in coexistence with MIMO radar," *IEEE Trans. Wireless Commun.*, vol. 19, no. 7, pp. 4727–4743, Apr. 2020.

[7] N. Su, F. Liu, and C. Masouros, "Secure radar-communication systems with malicious targets: Integrating radar, communications and jamming functionalities," *IEEE Trans. Wireless Commun.*, vol. 20, no. 1, pp. 83–95, Jan. 2021.

[8] A. R. Chiriyath, B. Paul, G. M. Jacyna, and D. W. Bliss, "Inner bounds on performance of radar and communications co-existence," *IEEE Trans. Signal Process.*, vol. 64, no. 2, pp. 464–474, Jan. 2016.

[9] H. Tataria, M. Shafi, A. F. Molisch, M. Dohler, H. Sjöland, and F. Tufvesson, "6G wireless systems: Vision, requirements, challenges, insights, and opportunities," *Proc. IEEE*, vol. 109, no. 7, pp. 1166–1199, Jul. 2021.

[10] Z. Yang, D. Li, N. Zhao, Z. Wu, Y. Li, and D. Niyato, "Secure precoding optimization for NOMA-aided integrated sensing and communication," *IEEE Trans. Commun.*, vol. 70, no. 12, pp. 8370–8382, Dec. 2022.

[11] T. Schenk, *RF Imperfections in High-Rate Wireless Systems: Impact and Digital Compensation*. Berlin, Germany: Springer-Verlag, 2008.

[12] P. Zhang, S. Chen, and L. Hanzo, "Two-tier channel estimation aided near-capacity MIMO transceivers relying on Norm-based joint transmit and receive antenna selection," *IEEE Trans. Wireless Commun.*, vol. 14, no. 1, pp. 122–137, Jan. 2015.

[13] J. Shen, H. Zhu, Y. Cai, B. Zhai, X. Wang, S. Chang, H. Cai, and M. Guo, "mmV2V: Combating one-hop multicasting in millimeter-wave vehicular networks," in *2022 IEEE 42nd International Conf. Distributed Computing Syst. (ICDCS)*, Oct. 2022, pp. 735–742.

[14] Y. Cai, H. Zhu, S. Chang, X. Wang, J. Shen, and M. Guo, "Peerprobe: Estimating vehicular neighbor distribution with adaptive compressive sensing," *IEEE/ACM Trans. Netw.*, vol. 30, no. 4, pp. 1703–1716, Aug. 2022.

[15] M. Richards, *Fundamentals of Radar Signal Processing*. New York, NY, USA: McGraw-Hill Education, 2014.

[16] S. Sesia, I. Toufik, and M. Baker, *LTE-The UMTS Long Term Evolution: From Theory to Practice*. 2nd ed. New York, NY, USA: Wiley, 2011.

[17] M. Kotaru, K. Joshi, D. Bharadia, and S. Katti, "Spotfi: Decimeter level localization using WiFi," in *ACM Conf. Special Interest Group Data Commun.*, Aug. 2015, pp. 269–282.

[18] I. S. Gradshteyn and I. M. Ryzhik, *Table of Integrals, Series, and Products, 7th ed.* New York, NY, USA: Academic, 2007.